COMPARISON OF SINGLE-SITE INTERPLANETARY SCINTILLATION SOLAR WIND SPEED STRUCTURE WITH CORONAL FEATURES

S. K. ALURKAR, P. JANARDHAN, and HARI OM VATS

Physical Research Laboratory, Ahmedabad-380 009, India

(Received 6 May, 1992; in revised form 28 August, 1992)

Abstract. Interplanetary Scintillation (IPS) Observations were made during the period 1984–1990 using a single radio telescope at 103 MHz situated at Thaltej (Ahmedabad), India. Solar wind speeds were estimated using a recently developed method based on matching the observed IPS spectra with model solar wind spectra for Kolmogorov turbulence. The best-fit speeds derived are traced back to a source surface, and average velocity maps are made for each year, averaging over a number of Carrington rotations. It is found that the resulting single-site, large-scale IPS speed structure agrees well with that derived from 3-site observations from earlier workers. The IPS speed structure during this period was compared with other coronal features. Nearly 85% of the observed high-speed regions were associated with coronal holes. At solar minimum, in 1986, a quasi-sinusoidal, narrow belt of slow solar wind was observed which matched well with the neutral line structure of the solar magnetic field and the belt of active centers. Near solar maximum, in 1990, the speed structure was chaotic, similar to that of the neutral line, with low speed regions appearing all over the source surface.

1. Introduction

It is well known that coronal structure, magnetic field, and solar wind speed structure strongly depend on solar activity. Using the Mauna Loa *K*-coronameter white-light observations over an entire solar cycle during 1965–1978, the slow evolution of large coronal holes was studied by Hundhausen, Hansen, and Hansen (1981). It was found that large coronal holes shrink in size during the ascending phase of the solar cycle, disappear from the poles at sunspot maximum and reappear near sunspot minimum. Association between solar wind streams observed at 1 AU and coronal holes was first established at UV and X-ray wavelengths using rockets and spacecraft (Krieger, Timothy, and Roelof, 1973; Nolte *et al.*, 1976; Broussard *et al.*, 1978). During the Helios 1 mission such relationships were shown for plasma streams observed between 0.3 and 1 AU (Burlaga *et al.*, 1978). Recently, Lindblad (1990) established individual stream-to-coronal hole relations for high-speed streams observed at 1 AU. Hoeksema, Wilcox, and Scherrer (1982) studied the changes in the structure of the heliospheric current sheet (HCS) during the early part of solar cycle 21 by applying a potential field model to the observed photospheric magnetic field. This work was followed by similar studies for the period 1978–1982 where it was found that the large-scale structure of the HCS evolved slowly during this period (Hoeksema, Wilcox, and Scherrer, 1983).

The three-dimensional global distribution of solar wind speed during the period 1973–1987 using 3-site interplanetary scintillation (IPS) observations was derived by Kojima and Kakinuma (1990). Among other things, they observed that the low-speed

Solar Physics **144:** 385–397, 1993.

regions were distributed along neutral lines. The long-term average behaviour of the three-dimensional solar wind was also studied over a solar cycle by Rickett and Coles (1991). They compared the IPS observations with coronal density and solar magnetic field and confirmed that during low solar activity the high-speed solar wind is associated with open-field, low-density coronal regions, whereas the slow wind is related to dense coronal regions around the neutral sheet.

The average distribution of the solar wind speed on the source surface near the photosphere and the line-of-sight component of the photospheric magnetic field were constructed by Hakamada (1987) and it was shown that the solar wind does not blow out uniformly from a coronal hole. A sinusoidal low-velocity belt around the equator on the source surface matched well with the brightness structure of the *K*-coronal intensity as well as with the distribution of closed field line regions in the photosphere.

The coronal hole morphology resulting from the Skylab mission in 1973–1974 showed that coronal holes were associated with open field line unipolar magnetic regions in the polar corona around solar activity minimum. On the contrary, solar active centers, over which the slower wind originates, are associated with closed magnetic field structures, like bipolar loops. The slower wind was confined to a near-equatorial activity belt 40° wide in which is embedded the HCS.

The Helios mission with plasma probes on board Helios 1 (1974–1986) and Helios 2 (1976–1980) collected a unique set of continuous data on plasma particles, magnetic fields, and plasma wave electric fields. One of the main findings of the Helios mission was regarding the basic structure of solar wind plasma streams. Near solar minimum in 1976, a two-stream pattern of very large amplitude, broad, quasi-periodic high-speed streams (HSS) was observed, which had resulted from two large, corotating streams originating from two fixed heliographic longitudes on opposite sides of the Sun (Schwenn *et al.*, 1978). Observing from a distance of 0.3 AU from the Sun, Helios 1 confirmed the association between a coronal hole and the HSS (Burlaga *et al.*, 1978).

The question of the instantaneous latitudinal gradient of solar wind speed was addressed by the Helios experiment. During solar minimum the two spacecraft were very close to each other in terms of radial distance, latitude and corotation time. It was found that two observations separated by more than 5° in latitude had a very small chance of encountering similar streams (Schwenn, 1991).

The development of the method of fitting model spectra to observed IPS spectra to determine solar wind velocities (Manoharan and Ananthakrishnan, 1990), requires a knowledge of the effects of variation in a number of parameters like power-law index, axial ratio of irregularities, source size, random velocity component and, most importantly, a knowledge of the smallest scale sizes present in the IPS. This scale size, known as the inner-scale, represents a spatial dissipative scale length below which there is little IPS power due to the absence of smaller irregularities. IPS observations (Coles, 1978; Scott, Coles, and Bourgois, 1983), and spacecraft experiments (Yakovlev *et al.*, 1980) showed that this scale size attenuates the IPS power spectrum at high temporal frequencies in a manner similar to the effects of the source size cut-off. Hence, differentiating between source size effects and effects caused by the inner-scale depend upon

reliable estimates of source sizes, which eventually came from very long baseline interferometry (VLBI) measurements. Once the medium has been calibrated to determine an inner-scale, reliable estimates of velocity can be obtained for spectra with good signal to noise ratio (S/N). A low S/N would cause the inner-scale to be undetermined due to the high-frequency portions of such spectra being contaminated by noise.

It has been recently shown that single-site IPS observations can also be used to derive reliable estimates of solar wind speed (Manoharan and Ananthakrishnan, 1990). Recent IPS observations with a large single antenna at 2, 8, and 22 GHz were used (Tokumaru *et al.*, 1991) to estimate solar wind velocities close to the Sun. These observations showed that the solar wind is considerably accelerated in the region between 10 and 30 solar radii (R_s).

2. Observations and Analysis

The observations reported here were carried out with the 10 000 m^2 dipole antenna array at Thaltej, near Ahmedabad, India. This antenna, operating at 103 MHz, is a filled aperture phased array, made up of 2048 fullwave dipoles. The array is divided into two halves, viz., the north and south. Each half comprises 32 transmission lines, each loaded with 32 dipoles, polarized horizontally in the N–S direction to form a correlation type interferometer observing sources at meridian transit. Thirty-two beams are formed by each half of the array using a beam-forming network, called the Butler matrix, which is essentially the analogue equivalent of a Fast Fourier Transform. These beams are deployed in declination and are each 1.8° N–S × 3.6° E–W and cover ± 30° of declination centered on the zenith. A pair of identical beams is connected, during each observation, to a correlation type receiver which yields sine and cosine quadrature outputs. The rapidly changing intensity fluctuations are picked up by a device called the scintillometer whose output is proportional to the square of the scintillation flux of the source. A full description of the system can be found elsewhere (Alurkar *et al.*, 1989). The physical area of the antenna was enhanced to 20 000 m^2 in 1989 by increasing the east–west dimensions of the array. The observations in 1990 therefore had a beam width of 1.8° N–S × 1.8° E–W.

The power spectrum for each observation of a source was computed by subtracting a Hanned spectrum of 10 min of data off-source from a Hanned spectrum of 10 min of data on-source. The on-source data were taken 5 min on either side of the transit time on each day from the available on-source data of about 15 min. All the spectra were normalized to the highest spectral density and had a frequency resolution before Hanning of 0.0813 Hz. The data were sampled at 20 Hz and digitized using a 12-bit, ± 5 V A/D converter (Alurkar *et al.*, 1989) and stored on a magnetic tape for analysis.

3. Results

Solar wind speeds were estimated using IPS measurements on about 10 radio galaxies simultaneously for the years 1984 through 1990, a period which covered the descending

phase of solar cycle 21 and minimum, ascending and maximum phases of solar cycle 22. The inferred speeds were traced back to the source surface about 2.5 R_s from the Sun along Archimedian spirals, assuming radial flow at constant speed. The IPS observations were made in the range 0.5 to 1.1 AU from the Sun. The constant speed assumption should be valid over this distance under generally undisturbed conditions. The IPS observation geometry is such that the measured speed is a weighted average of the components of the radial solar wind flow normal to the line of sight at the point of closest approach of the line-of-sight to the Sun. As a result of solar rotation and the Earth's revolution around the Sun, this IPS velocity point covers all heliolongitudes in about 27.3 days and a range of heliolatitudes in a year. An IPS source under observation reaches highest latitudes for only a short period of time when it is closest to the Sun. Thus, to get good coverage of heliolatitudes, velocity data for about 6 to 10 Carrington rotations were combined using a superposed-epoch analysis. The resulting average velocity map or V-map is a 2-dimensional projection on the source surface in heliolatitude and Carrington longitude. The antenna array used for these observations is a transit instrument and covers only one or two sources in the southern hemisphere.

The averaging of the solar wind speeds over Carrington rotations results in omitting streams having rotation periods different from 27.3 days. Also, streams lasting for only a day or two may be missed by the telescope as it observes any source only once every day. Such streams, if detected, are likely to be misinterpreted as coronal transients, or as shocks. This is because the time at which a stream is seen is critically dependant upon its time of departure from the Sun, as a given point in the sky will transit through the Thaltej radio telescope at a given time in the day. If the stream has not reached that point by that time then it will be seen only 24 hours hence, missed altogether, or seen only once and hence misinterpreted on the map as a transient. The accuracy of measurement of the solar wind speed was about ± 50 km s^{-1}. Therefore, speed enhancements of 100 km s^{-1} or more above the mean speed were considered to be high speeds.

The rectangular V-maps consist of ($15° \times 15°$) bins in latitude and longitude. To avoid lumping together in longitude the traced-back velocity data at high latitudes, the longitude resolution was smoothed by applying the correction $15° \times$ secant (latitude) at latitudes 45°, 60°, and 75°, as this ensures an approximately constant resolution of 15° on the sphere. Such a smoothed longitude resolution is satisfactory for IPS velocities measured between the helioequator and about 75° heliolatitudes (Rickett and Coles, 1991).

Average V-maps were plotted for velocity data from 1984 through 1990. Figures 1(a–d) show four such maps representing the descending phase of the solar activity cycle 21 in 1984, solar minimum in 1986, and ascending and maximum phases respectively in 1988 and 1990 of solar cycle 22. The Carrington rotation (CR) numbers and their corresponding year are indicated for each V-map. Three ranges of velocities are indicated on the map as: high speed, >550 km s^{-1}, medium speed, >450 km s^{-1} and ≤ 550 km s^{-1}, and slow speed, ≤ 450 km s^{-1}. The low-speed regions on each map have been hatched. It should be noted that during 1990 the latitudinal coverage extended down to $-70°$. This was due to the southern source 3C161 which could be observed

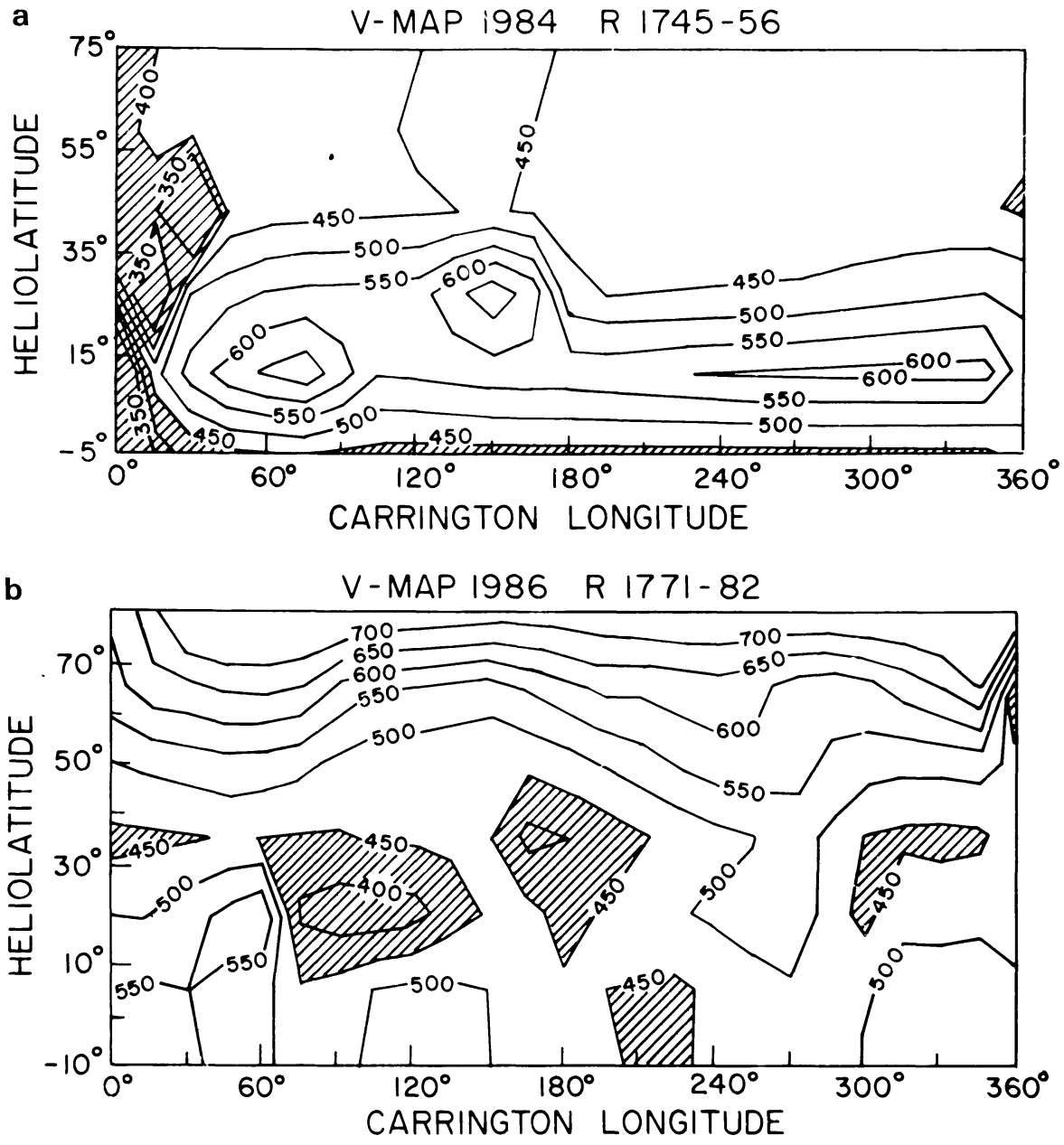

Fig. 1a, b.

Fig. 1a–d. Average V-maps from 1984 through 1990. While (a) and (b) show V-maps for the descending activity year 1984 of cycle 21 and the solar minimum year of 1986, respectively, (c) represents the ascending year 1988 of cycle 22. (d) Shows the V-map for 1990, the solar maximum year. The hatched regions indicate regions of slow solar wind (≤ 450 km s^{-1}).

with better S/N using the enhanced array. The main large-scale features of the solar wind speed structure are apparent in these single-site IPS V-maps. They indicate a belt of slow solar wind around the equator during solar minimum in 1986, and high-speed regions at latitudes higher than about 55° north. Of particular interest in the 1986 map are the regions of slow (≤ 450 km s^{-1}) flow in this belt at longitudes which coincide in position with the Giant Bipolar Magnetic Regions (GBMR) seen on the solar magnetic field

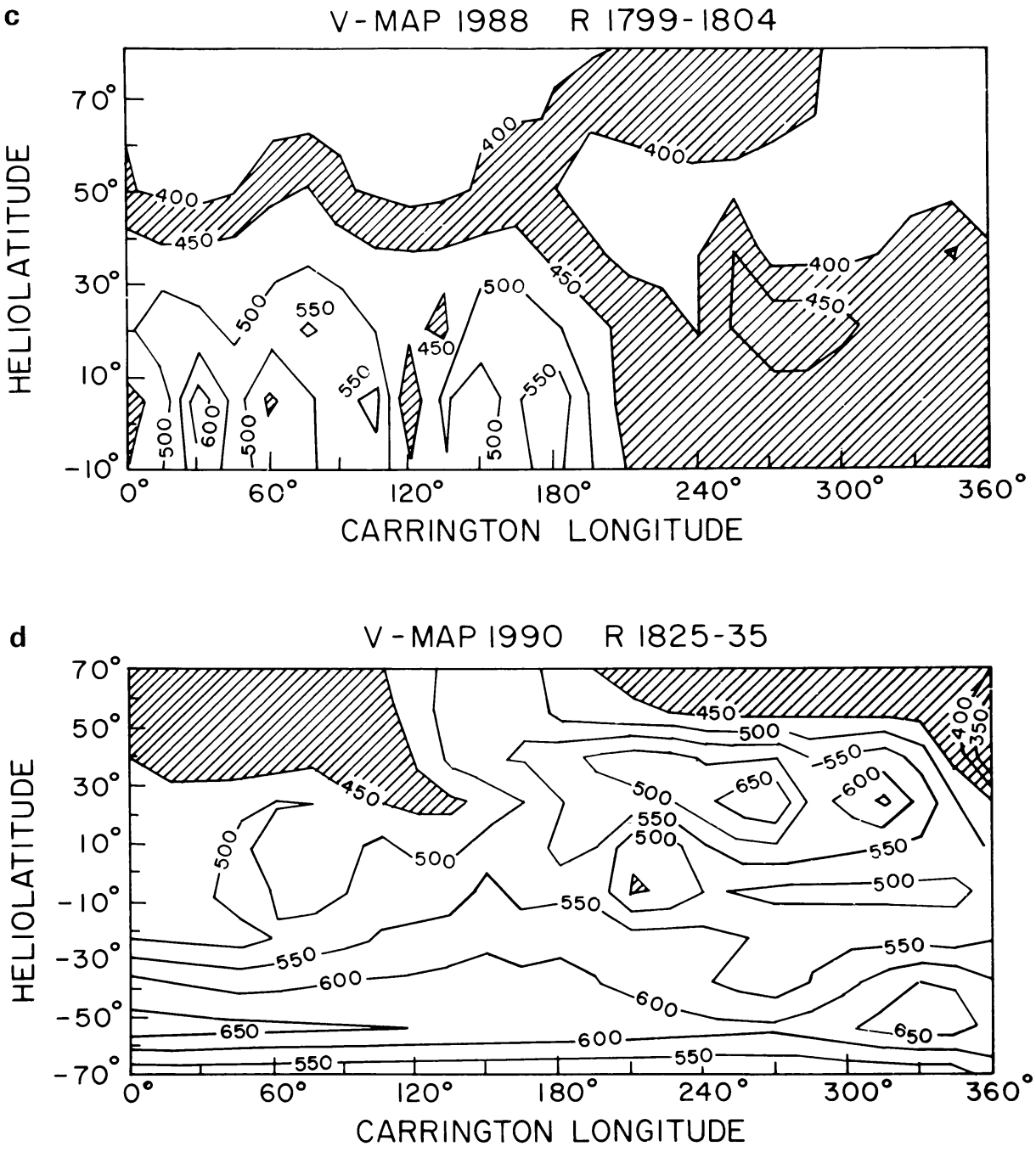

Fig. 1c, d.

synoptic charts for CRs from 1774 through 1777 (*Solar Geophysical Data*, April to July, 1986). These slow-speed regions were also reported by Kojima and Kakinuma (1990) from 3-site IPS data.

In Figures 2(a–c) are shown Carrington format maps of inferred coronal holes, observed photospheric magnetic field and predicted high-speed wind at 1 AU respectively for CR 1775 in 1986. These are Mount Wilson Observatory (MWO) data (Figure 4, Wang and Sheeley, 1990). The coronal field was determined by a current-free

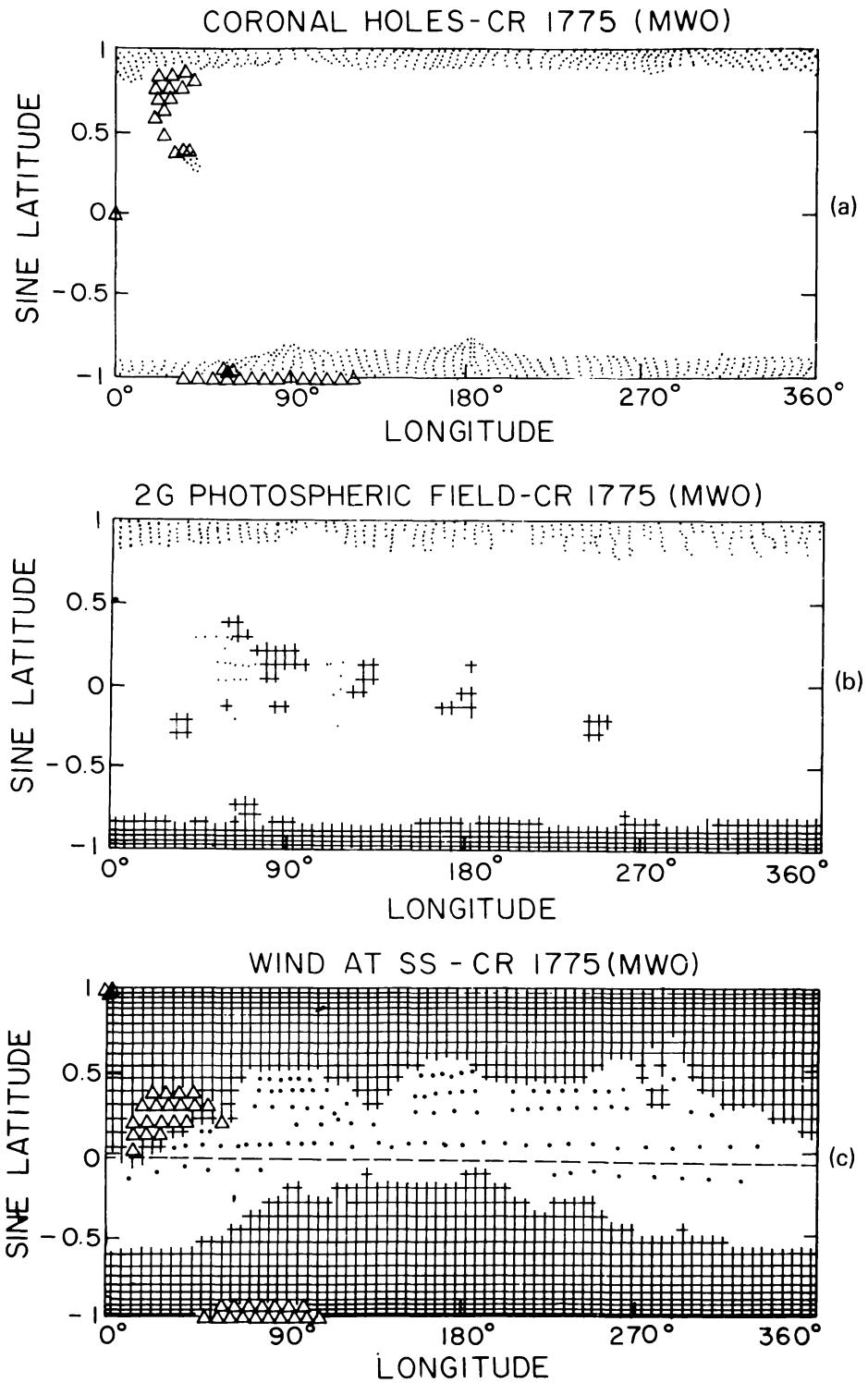

Fig. 2a–c. Carrington format maps for CR 1775 showing the distribution of (a) inferred coronal holes, (b) observed photospheric fields, and (c) predicted high speed wind at 1 AU. In (a) open field regions are indicated by dots while open triangles indicate the footpoints of Earth-directed field lines corresponding to regions of high (> 550 km s^{-1}) predicted wind speed. In (b) positive polarity field is shown by pluses for $B_r < 2$ G; negative polarity field is shown by blanks for $B_r > -2$ G and dots for $B_r \leq -2$ G. In (c) open triangles mark source surface locations of field lines for which the predicted wind speed is > 650 km s^{-1}, pluses indicate source surface regions with predicted speed between 550 and 650 km s^{-1}, while dots show negative-polarity field for which the speed is ≤ 550 km s^{-1} (Wang and Sheeley, 1990).

extrapolation of the observed photospheric flux distribution to a source surface at 2.5 R_s. In Figure 2(a) open-field regions (holes) are indicated by dotted areas while open triangles mark the footprints of Earth-directed field lines corresponding to regions of high (>550 km s^{-1}) predicted wind speed. Comparison of calculated hole configurations with corresponding He I λ10830 synoptic maps (Wang and Sheeley, 1990) have also shown excellent agreement. In Figure 2(b) positive-polarity photospheric fields are shown by pluses for $B_r < 2$ G while negative-polarity fields are shown by blanks for $B_r > -2$ G and dots for $B_r \leq -2$ G. In Figure 2(c) the open triangles mark source surface locations of field lines for which the predicted wind speeds are >650 km s^{-1} while pluses indicate source surface regions with predicted speed between 550 and 650 km s^{-1}. The dots show negative-polarity field for which the speeds are ≤ 550 km s^{-1}. Thus, the source surface neutral line runs between dotted and blank areas.

Due to insufficient IPS velocity observations, no V-map could be made for each solar rotation. However, in the case of long-lived solar structures such as polar coronal holes and photospheric fields observed at solar minimum, when relatively stable coronal conditions exist, broad features in an average V-map may be compared with them. During CR 1775 in 1986 Figure 2(c) indicates a predicted high-speed (>650 km s^{-1}) region (marked by triangles) from near the equator up to about 10°–20° N around 45° longitude, while Figure 2(a) indicates a large region of Earth-directed open field lines (marked by triangles) at a similar location with high predicted wind speeds. This region recurred during CRs 1776 and 1777 (MWO) data) and might have caused the high-speed region centered at 15° N latitude and 45° longitude as seen in Figure 2(c). A comparison with the V-map of 1986 shows a patch of high solar wind velocity centered about 20° N and around 45° longitude. The near-equatorial belt of low speed solar wind in this figure also compares well with that in Figure 1(b). It may be noted that the bipolar active centers of photospheric field during CR 1775 seen in Figure 2(b) lie in a narrow belt around the equator, which matches well with the observed and predicted slow-speed belts. This belt of bipolar active centers was clearly observed during the CRs 1774 through 1777 on the solar magnetic field synoptic charts of the Kitt Peak National Observatory (*Solar Geophysical Data*, April to July, 1986).

In Figures 3(a–d) average neutral magnetic lines for the same Carrington rotations corresponding to the years 1984, 1986, 1988, and 1990 are shown. These are based on the line-of-sight component of the photospheric magnetic field measured by the Stanford magnetometer and was calculated (Hoeksema, 1990) under the assumption that the coronal field is approximately a potential field and that the field at some height above the photosphere is completely radial. This model was first developed independently by Schatten, Wilcox, and Ness (1969) and Altschuler and Newkirk (1969). Later investigations (Adams and Pneuman, 1976; Altschuler *et al.*, 1976; Schulz, Frazier, and Boucher, 1978; Levine, 1982) demonstrated the basic validity of the model for predicting large-scale structure. In Figures 3(a–d) the calculated neutral line structure for each Carrington rotation (Hoeksema, 1990) was superimposed to produce a map showing the neutral line configuration lying along a wide band. A line was then drawn, by eye,

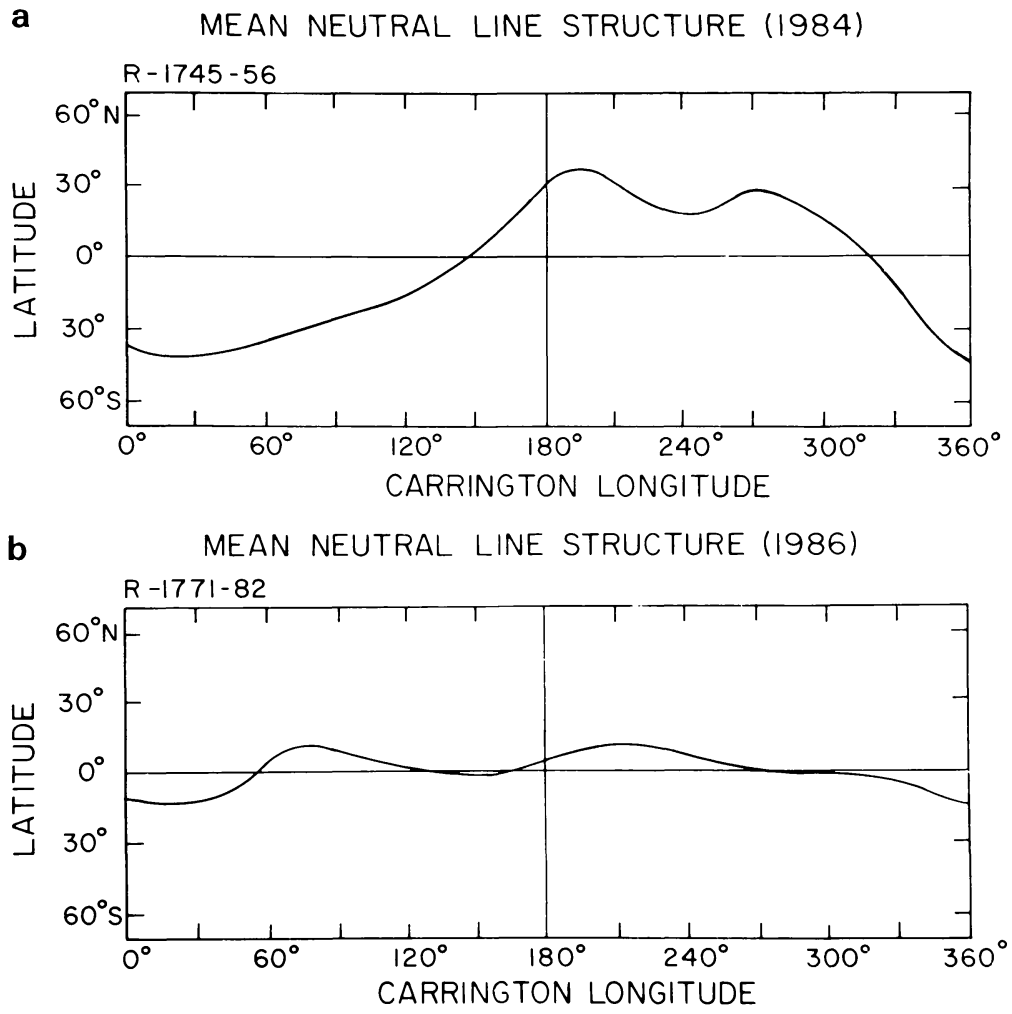

Fig. 3a, b.

Fig. 3a–d. Plots of the mean neutral line structure from 1984 through 1990 (Hoeksema, 1990), each averaged over the same Carington rotation numbers as the *V*-maps in Figures 1(a–d). The calculated neutral line structure for each Carrington rotation (Hoeksema, 1990) was superimposed to produce a map showing the neutral line configuration lying along a wide band. A line was then drawn, by eye, through the centre of this band to represent the mean neutral line structure for the rotations corresponding to those in the *V*-maps.

through the centre of this band to represent the mean neutral line structure for the rotations corresponding to those in the *V*-maps. As expected, during solar minimum in 1986 the average neutral line undergoes latitudinal excursions of about 15° on either side of the equator, corresponding to a nearly flat heliospheric current sheet (HCS). During the descending and ascending phases in 1984 and 1988 the HCS shows warps of higher amplitude. At maximum in 1990, however, the neutral line structure became very complex, with isolated regions of neutral magnetic field lines.

It is important to note that the narrow quasi-sinusoidal belt of slow solar wind around the equator in 1986 (Figure 1(b)) corresponds well to the distributions of neutral line in Figure 3(b) and brightness of white-light corona (Figure 6(d) in Rickett and Coles, 1991). Similar to the extension of the slow-speed belt to higher latitudes during the descending and ascending phases of solar activity, the widths of the brightness distri-

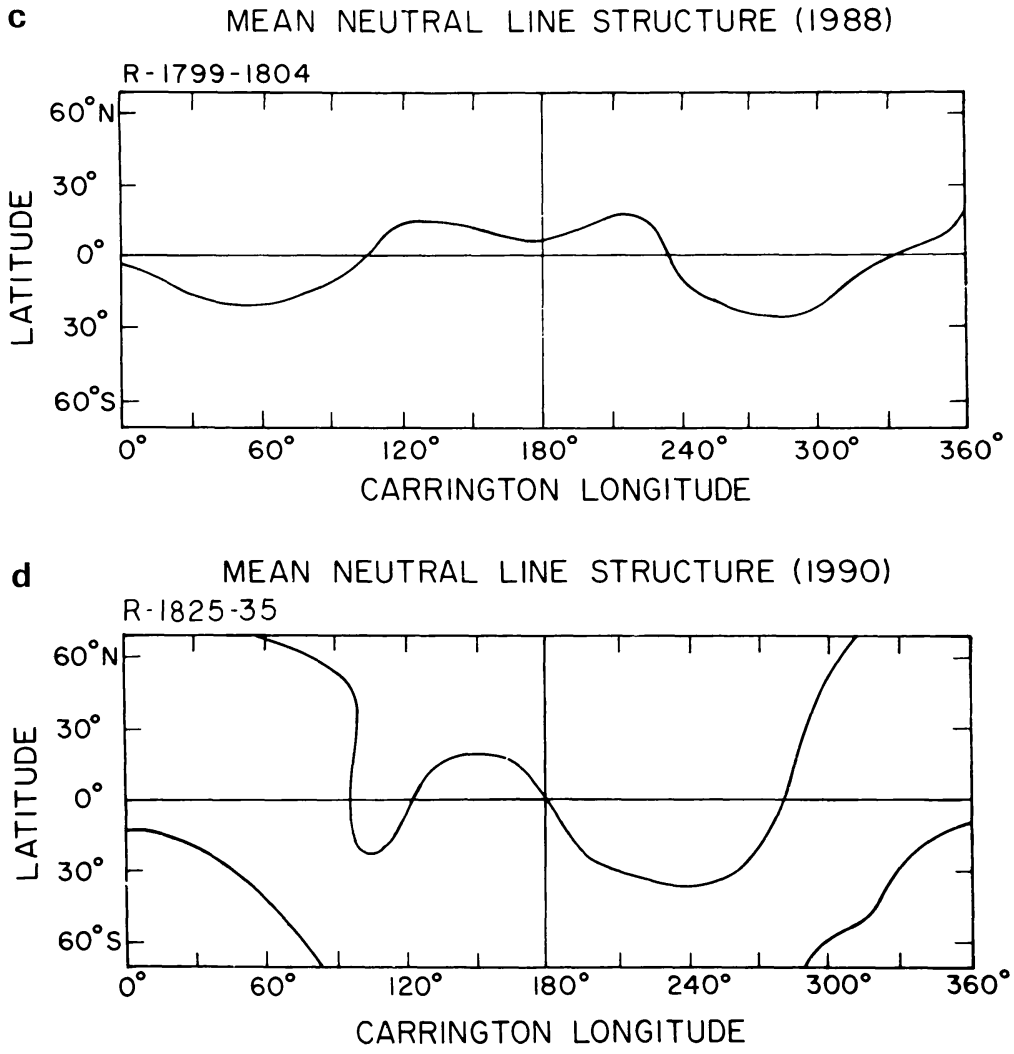

Fig. 3c, d.

bution of the white-light as well as that of the neutral line also vary during these phases (Wilcox and Hundhausen, 1983; Hoeksema, Wilcox, and Scherrer, 1983). At solar maximum, all the distributions – slow solar wind, neutral line and *K*-corona whitelight intensity – become very complex and their interrelation is not obvious. They spread all over the source surface and often form isolated regions, as in Figure 1(d) and Figure 3(d).

For stable coronal conditions in 1974, Hakamada (1987), using a potential field model, compared the 3-dimensional distribution (projected on the photosphere) of the coronal magnetic field with the average distribution of IPS wind speeds, projected on the photosphere along open field lines. He compared the high-speed regions with He 10830 Å coronal holes. The general shapes of high-speed flow and coronal hole regions were similar. However, the solar wind did not blow out uniformly from the coronal holes. He also observed that the sinusoidal structure of the slow-speed wind belt was similar to the distribution of the *K*-coronal brightness and the closed-field regions projected on the photosphere.

Using the three-site IPS observations, several high-speed streams (HSS) were shown to be associated with coronal holes (Sime and Rickett, 1978). The single-site IPS V-maps made for the period 1984 through 1990, except for 1989 when the Thaltej antenna array was being enhanced, indicated regions of high-speed streams ($V \geq 550$ km s^{-1}) which were associated with coronal holes (CHs). These latter were identified either by the He 10830 Å or by the Fe XIV 5303 Å line and published as Hα

TABLE I

Association between single-site recurrent HSS and coronal holes

Year	CR No. for V-map	IPS obs. of HSS ($V \geq 550$ km s^{-1})	HSS longitude (deg.)	CH 10830 Å[a] CR No.	CH 5303 Å[a] CR No.	Remarks
1984	1745–56	HS1	45	1745–50		
		HS2	75	1745–50		
		HS3	75	1745–50		
		HS4	135	–		Uncertain
		HS5	230	1748–49		
		HS6	345	1745–49		
1985	1757–70	HS1	70	1757–58		
		HS2	130	1769		
		HS3	150	1760–63		
		HS4	260	1762–65		
1986	1771–82	HS1	28	1771–75		
		HS2	32			High-lat. coronal region
1987	1785–96	HS1	30	–	1786	High-lat. coronal region
		HS2	75			Uncertain
		HS3	105	1789–93	1786	
		HS4	165	–		Uncertain
		HS5	225	–	–	
		HS6	300		1785–86	
		HS7	34.5		1785–86	
1988	1799–1804	HS1	30	–	–	Uncertain
		HS2	135			
		HS3	160	1799–1801		
		HS4	210	–	1799–1801	
		HS5	280	–	1799–1801	
		HS6	315	–	1799–1801	
1990	1825–35	HS1	130	–	1833	North polar lat.
		HS2	165			
		HS3	180	–	1833–35	
		HS4	195	1833–35	–	
		HS5	250	–	1833	
		HS6	250	–	1833	
		HS7	300	1833–35	–	
		HS8	315	1833–35	–	

[a] Only those coronal holes covering 15° or more in both heliolatitude and longitude are considered.

solar synoptic charts for each CR in the *Solar Geophysical Data* reports. Only those streams which lasted for one or more rotations were considered. The associated CHs had approximately comparable positions in heliolatitude and longitude coordinates with those of the HSS with CH extensions of about 30°. Table I summarizes this comparison study. A total of 34 HSS were identified on the V-maps, of which only 4 could not be associated with any CH. The reason for this could not be ascertained.

4. Discussion

It is seen in the preceding section that the main large-scale features, such as distribution of the low- and high-speed regions on single-site IPS V-maps, their spatial variation with solar activity cycle, and correspondence to solar magnetic field variations are in general agreement with those derived from 3-site IPS V-maps (Kojima and Kakinuma, 1990; Rickett and Coles, 1991).

Around solar minimum in 1986 the slow solar wind ($V \leq 450$ km s^{-1}) was confined to a narrow belt of width 25°–30° around the equator, at a time when the neutral magnetic line also followed the equator closely. Bruno *et al.* (1986) compared solar wind data taken by the Helios 1, 2 and IMP spacecraft during 1976–1977 with the heliospheric current sheet positions. They found that the slow-speed wind was confined within $\pm$ 20° of the latitudinal separation of the current sheet, beyond which high-speed wind existed. This slow wind flow, between two broad high-speed regions, is found to be associated with minima in proton temperature and helium content and a maximum in proton density. This result was based on a superposed epoch analysis of 23 carefully selected sector boundaries (Gosling *et al.*, 1981) observed by IMP6/7/8 at 1 AU (Borrini *et al.*, 1981). The slow-speed flow may emerge from coronal streamers, which extend out to 10 R_s; the streamers, in turn, are thought to emanate from above bipolar regions having closed-loop systems.

As seen from the V-maps in Figures 1(c) and 1(d) during high solar activity we infer that there is lot of slow wind away from the solar equator. This flow is probably emitted from coronal regions far away from coronal streamers and is not associated with them. It may be possible that other small-scale interstream flows exist in coronal regions located above photospheric regions of high activity and magnetic fields (Schwenn, 1991).

Acknowledgements

We thank all the staff members of the Radio Astronomy group for their help and cooperation. In particular we are grateful to Drs P. K. Manoharan, and S. Ananthakrishnan, TIFR Ooty, for allowing us to use their software for single-site velocity determination. We are also grateful to Dr N. R. Sheeley Jr. of NRL and Dr J. T. Hoeksema of Stanford, for providing us with plots of coronal holes, photospheric fields and predicted solar wind speed for CR 1775 and neutral magnetic line plots respectively. Financial assistance for this work came from the Departments of

Space and Science and Technology, Government of India and the Special Foreign Currency (SFC) project No. NA87AA-D-ER046 under an Indo-US collaboration.

References

Adams, J. and Pneuman, G. W.: 1976, *Solar Phys.* **46**, 185.
Altschuler, M. D. and Newkirk, G., Jr.: 1969, *Solar Phys.* **9**, 131.
Altschuler, M. D., Levine, R. H., Stix, M., and Harvey, J. W.: 1976, *Solar Phys.* **51**, 345.
Alurkar, S. K., Bobra, A. D., Nirman, N. S., Venat, P., and Janardhan, P.: 1989, *Ind. J. Pure Appl. Phys.* **27**, 32.
Borrini, G., Gosling, J. T., Bame, S. J., Feldman, W. C., and Wilcox, J. M.: 1981, *J. Geophys. Res.* **86**, 4565.
Broussard, R. M., Sheeley, N. R., Jr., Tousey, R., and Underwood, J. H.: 1978, *Solar Phys.* **56**, 161.
Bruno, R., Villante, U., Bavassano, B., Schwenn, R., and Mariani, F.: 1986, *Solar Phys.* **104**, 431.
Burlaga, L. F., Ness, N. F., Mariani, F., Bavassano, B., Villante, U., Rosenbauer, H., and Schwenn, R., Harvey, J.: 1978, *J. Geophys. Res.* **83**, 5167.
Coles, W. A.: 1978, *Space Sci. Rev.* **21**, 411.
Gosling, J. T., Borrini, G., Ashbridge, J. R., Bame, S. J., Feldman, W. C., and Hansen, R. T.: 1981, *J. Geophys. Res.* **86**, 5438.
Hakamada, K.: 1987, *J. Geophys. Res.* **92**, 4339.
Hoeksema, J. T.: 1990, *An Atlas of Photospheric Magnetic Field Observations, 1985–1990*, Rep. CSSA-ASTRO-91–01, Vol. 2.
Hoeksema, J. T.Wilcox, J. M., and Scherrer, P. H.: 1982, *J. Geophys. Res.* **87**, 10331.
Hoeksema, J. T., Wilcox, J. M., and Scherrer, P. H.: 1983, *J. Geophys. Res.* **88**, 9910.
Hundhausen, A. J., Hansen, R. T., and Hansen, S. F.: 1981, *J. Geophys. Res.* **86**, 2079.
Kojima, M. and Kakinuma, T.: 1990, *Space Sci. Rev.* **53**, 273.
Krieger, A. S., Timothy, A. F., and Roelof, E. C.: 1973, *Solar Phys.* **23**, 123.
Levine, R. H.: 1982, *Solar Phys.* **79**, 203.
Lindblad, B. A.: 1990, *Astrophys. Space Sci.* **170**, 55.
Manoharan, P. K. and Ananthakrishnan, S.: 1990, *Monthly Notices Roy. Astron. Soc.* **244**, 691.
Nolte, J. T., Krieger, A. S., Timothy, A. F., Gold, R. E., Roelof, E. C., Vaiana, G., Lazarus, A. J., Sullivan, J. D., and MacIntosh, P. S.: 1976, *Solar Phys.* **46**, 303.
Rickett, B. J. and Coles, W. A.: 1991, *J. Geophys. Res.* **96**, 1717.
Schatten, K. H., Wilcox, J. M., and Ness, N. F.: 1969, *Solar Phys.* **6**, 442.
Schulz, M., Frazier, E. N., and Boucher, D. J., Jr.: 1978, *Solar Phys.* **60**, 83.
Schwenn, R.: 1991, in R. Schwenn and E. Marsch (eds.), *Physics of the Inner Heliosphere*, Springer-Verlag, Berlin.
Schwenn, R., Montgomery, M. D., Rosenbauer, H., Miggenrieder, H., and Mühlhäuser, K. H.: 1978, *Geophys. Res.* **83**, 1011.
Scott, S. L., Coles, W. A., and Bourgois, H.: 1983, *Astron. Astrophys.* **123**, 207.
Sime, D. G. and Rickett, B. J.: 1978, *J. Geophys. Res.* **83**, 5757.
Tokumaru, M., Mori, H., Tanaka, T., Kondo, T., Takaba, H., and Koyama, Y.: 1991, *J. Geomagn. Geoelectr.* **43**, 619.
Wang, Y. M. and Sheeley, N. R., Jr.: 1990, *Astrophys. J.* **365**, 372.
Wilcox, J. M. and Hundhausen, A. J.: 1983, *J. Geophys. Res.* **88**, 8095.
Yakovlev, O. I., Efimov, A. I., Razmanov, V. M., and Shtrykov, V. K.: 1980, *Soviet Astron.* **24**, 454.